CLUSTERING OF INTENSE STRUCTURES IN ISOTROPIC TURBULENCE: NUMERICAL AND EXPERIMENTAL EVIDENCE

Frédéric Moisy
Fluides, Automatique et Systèmes Thermiques, Bât. 502, 91405 Orsay Cedex (France)
moisy@fast.u-psud.fr

Javier Jiménez
School of Aeronautics, U. Politécnica, 28040 Madrid (Spain)
Centre for Turbulence Research, Stanford University (USA)
jimenez@torroja.dmt.upm.es

Abstract

The spatial distribution of intense structures in isotropic turbulence is studied from numerical and experimental data. Box-counting of the intense vorticity and strain rate sets gives evidence of a strong clustering at intermediate scales, from which a possible fractal dimension can be defined. Algebraically distributed free intervals between intense velocity derivative from experimental time series confirms this self-similar clustering at larger Reynolds numbers, but without further specifying its dimensionality.

Keywords: Turbulence, Clustering, Box-counting, Fractals, Dimension

1. Introduction

Regions of high levels of dissipation and of vorticity in turbulent flows, such as vortex sheets and tubes, have been observed and characterized for a long time from numerical simulations. They result in highly non-Gaussian statistics of the velocity increments, which may depend both on the geometry of the individual structures, on their size distribution and on their spatial distribution at larger scales. Vortex tubes probably arise from stretched vortex layers formed at earlier time (Passot *et al.* 1995), and it is in those layers, and in the periphery of the vortex tubes, that high levels of energy dissipation are concentrated.

Intense objects are often treated as being randomly distributed in space. With this assumption, Hatakeyama & Kambe (1997) obtained inertial range scaling from an assembly of random Burgers' vortices. However, evidence from numerics is inconsistent with a fully random distribution. Worms seem to accumulate in the interface between largely empty large-scale eddies (Jiménez *et al.* 1993), leading to an apparent inertial-scale clustering of intense vortices (Porter, Woodward & Pouquet 1997). Box-counting methods have been used by Moisy & Jiménez (2004) to further characterize this clustering.

Experimentally, spatial distributions can be inferred from waiting times between intense events recorded in one-point time series. The results of pressure measurements by Abry *et al.* (1994) showed algebraically-distributed waiting times, for inertial separations, between pressure drops marking large coherent vortices, suggesting self-similar clustering. Belin *et al.* (1996) and Mouri, Hori & Kawashima (2002) gave evidence, from one-point velocity time series, of the clustering of intense velocity gradients, which was shown to be self-similar by Camussi & Guj (1999) and Moisy (2000).

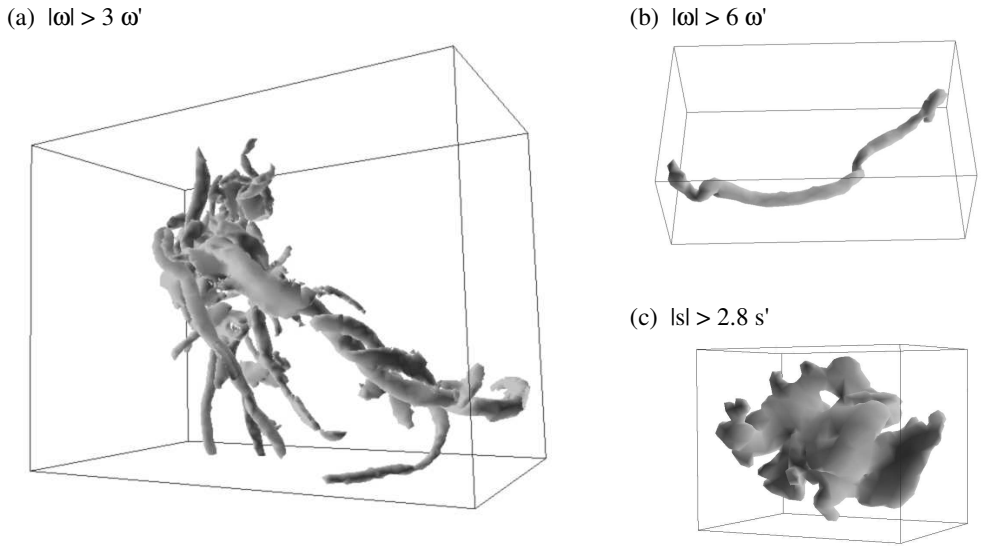

Figure 1. Structures of intense vorticity (a, b) and intense strain rate (c).

2. Box-counting of intense sets from numerical data

Examples of structures of intense vorticity and intense strain rates are shown in figure 1 (Moisy & Jiménez 2004). Here, a *structure* simply refers to a connected volume satisfying a thresholding criterion, $|\omega| \geq \tau\omega'$ or $|s| \geq \tau s'$, where the primes denote the rms values, with $\omega'^2 = 2s'^2 = \epsilon/\nu$ (ϵ is the energy dissipation rate and ν the kinematic viscosity). These structures have been extracted from numerical simulations of forced isotropic turbulence at $Re_\lambda = 168$ (Jiménez *et al.* 1993). The resolution is 512^3 collocation points, with periodic boundary conditions. The box size is 760η and the integral scale L_0 is around 1/4 of the box size, providing a scale separation of $L_0/\eta \simeq 200$.

The vorticity structures essentially show ribbons for moderate thresholds, and long filamentary tubes (figure 1b) for higher ones. The biggest structures associated to a moderate vorticity threshold show patterns resulting from the interaction of an intense vortex tube with surrounding weaker tubes, as in figure 1a. Very large thresholds only show smaller tubes, probably parts of the larger ones observed at lower thresholds, but no sheets or ribbons. The situation is different for the strain rate structures, for which both moderate and large thresholds show essentially sheets or ribbons. For low thresholds, the selected objects show intricate sponge-like patterns (figure 1c), or assemblies of sheets and ribbons. Increasing the threshold results in structures more like isolated sheets or ribbons.

In order to characterize the distribution of these structures in space, we begin by applying the classical method of box-counting to the sets of points of intense vorticity and strain rate magnitude. The computational domain is divided into cubical boxes of side r, and the number $N(r)$ of boxes containing some point of the set is counted. In the case of a pure fractal set of dimension D, the number of boxes would follow a power law $N(r) \sim r^{-D}$. In real systems this relation only holds in a restricted range of scales between a large- and a small-scale cutoff.

Figure 2 shows box counts for the sets of points of high vorticity, $N_\omega(r)$, for different values of the threshold. Similar results are obtained for the box count of the strain rate sets. The curves approach $N_\omega(r) \sim r^{-3}$ as $r \to L$, in which case both the high-dissipation and the high-enstrophy sets look as a single solid object. At the small-scale end, $r \approx \eta$, the slopes also increase, reflecting the compactness of the objects at scales which are small enough for viscous effects to be important. For $r \ll \eta$ both sets should look as collections

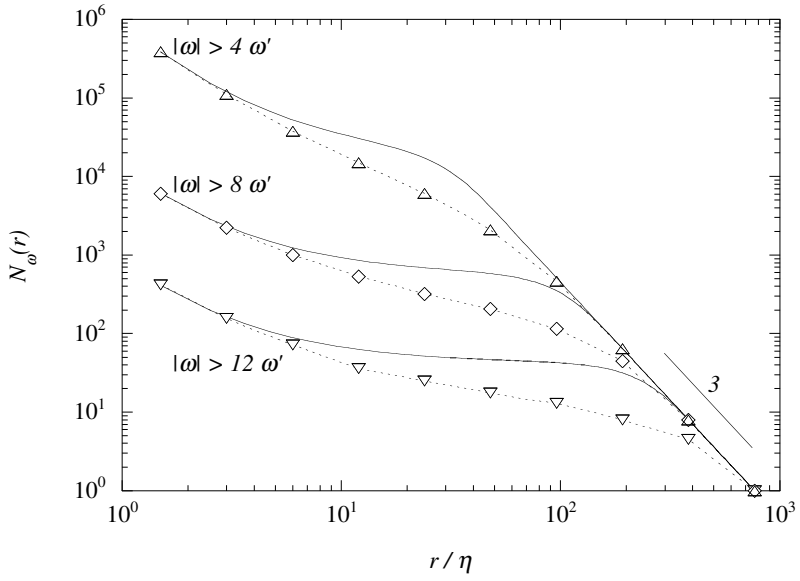

Figure 2. Symbols: Number of boxes of size r covering the vorticity sets, for the thresholds $|\omega| \geq 4$, 8 and 12 ω'. —, Box counts for sets of Poisson-distributed balls of the same total volume (data from the numerical simulation).

of small solid volumes, and one should expect the box counts to behave as $N(r) \simeq r^{-3}$. For intermediate scales, $\eta \ll r \ll L$, the box counts show a continuous evolution with the threshold, and none of the curves displays a real power-law range.

In order to interpret these box counts, it is of interest to compare them with box counts of sets with no clustering. If we consider a set of Poisson-distributed balls of radius δ, the expected number of covering boxes is

$$N_0(r) = \left(\frac{L}{r}\right)^3 \left(1 - \exp[-(r+\delta)^3/r_0^3]\right), \tag{1}$$

where r_0 is the mean distance between the balls. Together with the box-counts of figure 1 are plotted the best fits given by equation (1), using the constraint that the actual sets and the Poisson sets have the same volume, i.e. $N_0(r) \simeq N_\omega(r)$ for $r \to \eta$. Clearly the actual box counts are not described well by the assumption of Poisson-distributed balls. The actual number of covering boxes $N_\omega(r)$ is found to be significantly smaller than $N_0(r)$ for the central range $10\eta < r < 200\eta$, implying that the regions of high vorticity are concentrated on a smaller fraction of space than the random balls.

The clustering of the intense vorticity and strain rate sets for intermediate scales can be further characterized by introducing a local scaling exponent, defined as the logarithmic slope $D(r) = -\ln N(r)/dr$. Since one must recover the trivial exponent $D = 3$ at both large and small scales, one may expect the minimum slope, D^*, to provide a useful measure of the dimensionality of the clustering. In the ideal case of objects distributed in space with a fractal dimension D, we should expect $D^* \to D$ in the limit of very large scale separation $\eta \ll r \ll L$. For finite scale separation, both the large- and the small-scale contamination tend to increase the observed minimum D^*, which therefore only represents an upper bound for the possible fractal dimension.

This minimum slope D^* is plotted in figure 3 as a function of the threshold for the vorticity and the strain rate sets. Both D^*_ω and D^*_s decrease as the threshold increases, and none of them shows a plateau on which to define a threshold-independent dimension. The sets associated to typical fluctuations, $|\omega| \simeq \omega'$ and $|s| \simeq s'$, have dimensions of about 2.5, suggesting that regions of typical dissipation and enstrophy levels

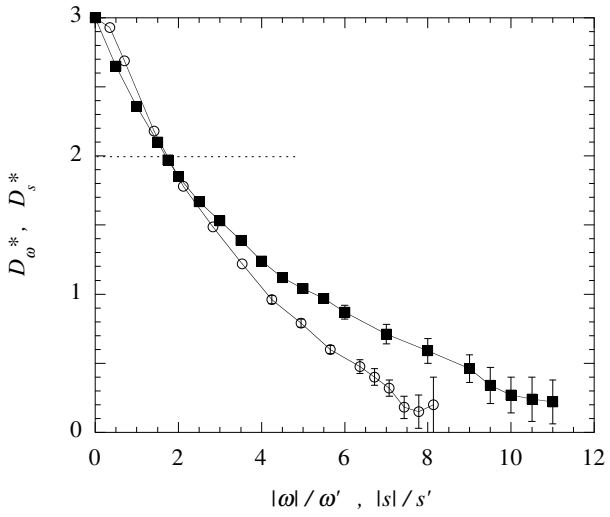

Figure 3. Minimum of the local slope of box counts as a function of the threshold, for the vorticity (■) and the strain rate (○) fields. The intersections of these curves with $D = 2$ (horizontal dashed line) indicate the thresholds above which sets of negative dimension are expected from experimental one-point measurements (see § 3).

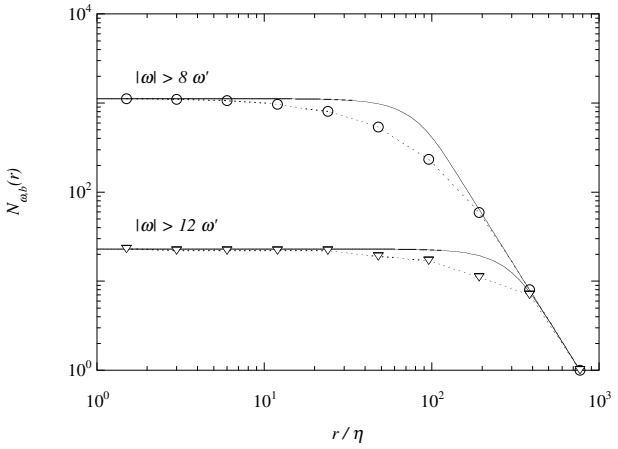

Figure 4. Symbols: Number of boxes of size r covering the set of baricenters of the vorticity structures, for the thresholds $|\omega| \geq 6$ and 12 ω'. —, Box counts for sets of Poisson-distributed points.

are wrinkled sheets, in qualitative agreement with other indirect estimates (Sreenivasan 1991; Sreenivasan & Antonia 1997).

Since the vorticity and strain rate sets considered here are a collection of structures as those shown in figure 1, two contributions are expected for the box counts. For scales smaller or of the order of the structures size, the box counts essentially describe the geometry and the size distribution of the structures, while for larger scales the box counts is more sensitive to their spatial distribution. Since we are interested in the

clustering of the intense structures, one may separate the latter contribution from the global box-counting, by replacing each structure by a single point located at its baricenter, and applying the box-counting method to the resulting point sets. This procedure is only valid in the limit of very large threshold, for which the mean distance between structures is expected to be much larger than the structure size.

Figure 4 shows the box counts $N_b(r)$ for the set of baricentres of the intense vorticity structures for two values of the threshold. As before, the scaling $N_b(r) \sim r^{-3}$ for large scales indicates the homogenous covering at large scales. At small scales, $N_b(r)$ saturates at the total number of structures, as expected for a set of points. The cross-over between the small-scale plateau and the large-scale decrease occurs at the typical distance r_0 between structures, which depends on the threshold.

These box-counts may be compared to that of Poisson-distributed points, by taking $\delta = 0$ in equation (1). As for the global box-counting, the actual curves are well below the Poisson law, indicating that the points are concentrated in a smaller fraction of space than for the random set. This clustering fraction is maximum for scales in the inertial range, and takes values around 0.5. Similar results are obtained for the clustering of intense strain rate structures. One may conclude that the clustering effect shown in figure 2 is not only an effect of the intense vorticity field being concentrated into structures, but also that the structures themselves are concentrated into clusters.

3. Clustering of intense events from experimental data

An issue raised by the previous observations in the low Reynolds number numerical simulations is whether the clustering of intense regions is still present at higher Reynolds number, and whether a range of scales exists for which this clustering is self-similar.

The decrease of the dimension D^*_α as the threshold is increased in figure 3 has important consequences for experiments for which only one-point measurements are available. From those measurements, the clustering of intense regions may be characterized from the distribution of the free intervals between successive intense events (Belin *et al.* 1996; Moisy 2000; Mouri, Hori & Kawashima 2002). For a fractal set of points of dimension $0 < d < 1$ with self-similar clustering, the distribution of the free intervals Δx decays as Δx^{-1-d} (Feder 1988). However, for large enough thresholds, figure 3 shows that both the vorticity and the dissipation fields concentrate into sets of dimension $D < 2$. As a consequence, the corresponding sets defined from one-dimensional cuts, as obtained from one-point time series with the use of the Taylor's hypothesis, should have a dimension $d = D - 2 < 0$, and are therefore almost surely empty. Only the presence of a small-scale cutoff, imposed by the Kolmogorov length scale or by the probe resolution, ensures that the one-dimensional sections are not empty.

Distributions of the free intervals Δx between successive intense velocity derivatives have been computed from experimental time series. The data are from a low temperature helium experiment, in which a large range of microscale Reynolds numbers can be spanned in very controlled conditions, Re_λ from 150 up to 2000 (Zocchi *et al.* 1994; Moisy, Tabeling & Willaime 1999). The flow takes place in a cylinder and is driven by two rotating disks equipped with blades, 20 cm in diameter and spaced 13 cm apart. Velocity measurements were carried out using a hot wire anemometer, and the Taylor hypothesis has been used to convert temporal fluctuations into spatial ones.

Figure 5 shows the probability density function $p(\Delta x/\eta)$ of the free intervals between intense longitudinal velocity derivative, $|\partial_x u| \geq \tau(\partial_x u)'$, for 3 different values of the threshold τ, for $Re_\lambda = 1300$. As before, the prime denotes the rms value, which is related to the mean energy dissipation rate using the assumption of isotropy, $(\partial_x u)'^2 = 2s'^2/15 = \epsilon/15\nu$. Note that, since only the longitudinal component of the velocity can be measured in the experiment, the intense longitudinal velocity derivatives are expected to trace essentially the intense strain rate regions rather than the intense vorticity regions. With this approximation, the quantity $(\partial_x u)^2$ has been extensively used as a one-dimensional surrogate for the local energy dissipation rate $\epsilon(\mathbf{x})$ (Sreenivasan 1991).

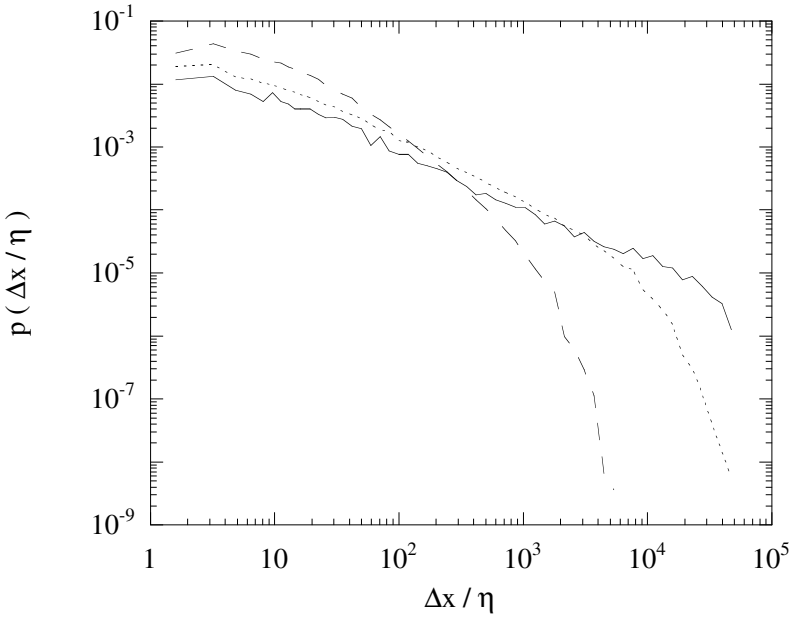

Figure 5. Probability density functions of the free intervals between intense velocity derivative $|\partial_x u|$ from the experimental time series, for $Re_\lambda = 1300$. They have been computed using logarithmic bins to ensure an acceptable number of events in the bins corresponding to the highest intervals. Thresholds: $--$, $2(\partial_x u)'$; ..., $5(\partial_x u)'$; —, $8(\partial_x u)'$.

For sufficiently large threshold, the pdfs show a clear power law decay over a significant range of scales, starting from the dissipative range, $\Delta x \simeq 3\eta$, up to a large scale cutoff, of order of $10^3 - 10^4\eta$, that depends on the threshold. This algebraic decay confirms that the intense events do not appear randomly in space, but tend to form self-similar clusters with no characteristic scale. Beyond the large scale cutoff, the pdfs decay approximately exponentially, indicating statistically uncorrelated events at large scales. The poorly defined scaling law for moderate threshold probably originates from the increasing contribution from the exponential decay, that may contaminate intermediate scales.

The exponent μ of the power law decay, $p(\Delta x) \sim \Delta x^{-\mu}$, is plotted as a function of the threshold τ in figure 6a. It is found to slightly decrease from values larger than 1, and saturates toward approximately 1 for large threshold. This trend is consistent with the fractal dimension D^* determined from the numerical simulations, that takes values less than 2 for large enough threshold (see figure 3). As a consequence, the law $p(\Delta x) \sim x^{-1-d}$ with $d = D - 2$ does not hold any more for $d < 0$, and the distributions collapse towards the single curve $p(\Delta x) \sim \Delta x^{-1}$ for sufficiently large threshold. Similar observations have been reported for the free intervals between intense scalar fronts in turbulent mixing (Moisy *et al.* 2000).

In figure 6b is plotted the exponent μ_∞, obtained in the limit $\tau \gg 1$, as a function of Re_λ, indicating that the power law $p(\Delta x) \sim \Delta x^{-1}$ is robust for sufficiently large Reynolds numbers, $Re_\lambda > 400$. This asymptotic exponent μ_∞ is found to increase from 0.5 to approximately 1 for $Re_\lambda < 400$. It must be noted that values of μ less than 1 for low Reynolds numbers can not be interpreted in the frame of the law $p(\Delta x) \sim x^{-1-d}$ for an exact fractal set of points of dimension d, and probably results from finite scaling effects.

These experimental distributions confirm that the intense events appear within self-similar clusters, and cannot be considered as randomly distributed. This is consistent with the clustering of the intense dissipation

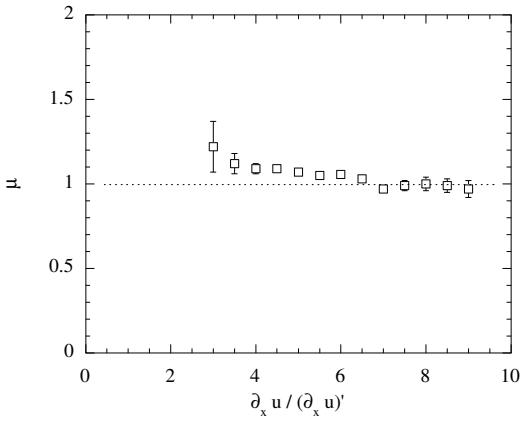

Figure 6a. Exponent μ of the power law from the distribution of free intervals between intense velocity derivative, $p(\Delta x) \sim \Delta x^{-\mu}$, as a function the threshold (data from the figure 5).

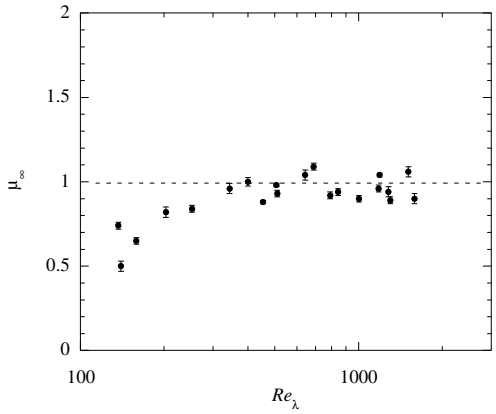

Figure 6b. Exponent μ in the limit of large threshold, $\tau \gg 1$, as a function of Re_λ.

events observed in the low Reynolds numbers simulations, but the one-dimensional cut in the experiment does not allow to further characterize the dimensionality of this clustering.

4. Discussion and conclusion

Three-dimensional box-counting from numerical simulations, and pdf of free intervals from experiments, gave evidence that the intense regions in isotropic turbulence, in the form of vortex sheets or tubes, tend to form clusters of inertial range extent. The dynamics of formation of the small scale structures from the instability of stretched shear layers at larger scales is probably the reason for this phenomenon. One may speculate that, for large Reynolds numbers, this process may repeat at different scales, leading to the observed self-similar clustering.

It is important to note that algebraic distributions for free intervals are not a trivial consequence of the self-similarity of the velocity field itself. Orey (1970) rigorously established that level sets from a Gaussian process with a power-law spectrum, $E(k) \sim k^{-n}$ with $1 < n < 3$, lead to fractal set of point of dimension $d = (3-n)/2$. In the case of the Kolmogorov spectrum, $n = 5/3$, this relation yields $d = 2/3$, and pdf of free intervals between iso-values of the velocity should decay as $p(\Delta x) \sim \Delta x^{-d-1} \sim \Delta x^{-5/3}$. Although turbulent velocity fluctuations are not Gaussian, the experimental results of Praskovsky *et al.* (1993) and Scotti, Meneveau & Saddoughi (1995) were in good agreement with Orey's theorem. However, it is clear that a fractal velocity field does not imply that the derivative fields are also fractal, and thus provides no insight into the spatial distribution of intense structures. Orey's theorem does not hold for the vorticity or dissipation fields, which have a spectrum $k^2E(k) \sim k^{1/3}$. For instance, a Gaussian process with power-law spectrum and random phase has sets of iso-derivatives that are randomly distributed. One may conclude that the clustering of intense structures with a distribution of free intervals as $p(\Delta x) \sim \Delta x^{-1}$ is not a trivial consequence of the Kolmogorov spectrum, but is a true intermittency effect, that reveals the hierarchical organization of the small scale structures in turbulence.

The authors are indebted to P. Tabeling and H. Willaime for the use of the experimental data and for fruitful discussions.

References

ABRY, P., FAUVE, S., FLANDRIN, P. & LAROCHE, C. 1994 Analysis of pressure fluctuations in swirling turbulent flows. *J. Phys. II France* **4**, 725–733.

BELIN, F., MAURER, J., TABELING, T. & WILLAIME, H. 1996 Observation of intense filaments in fully developed turbulence. *J. Phys. II France* **6**, 573–583.

CAMUSSI, R. & GUJ, G. 1999 Experimental analysis of intermittent coherent structures in the near field of a high Re turbulent jet flow. *Phys. Fluids* **11**, 423–431.

FEDER, J. 1988 *Fractals*, Plenum, New York.

HATAKEYAMA, N. & KAMBE, T. 1997 Statistical laws of random strained vortices in turbulence. *Phys. Rev. Lett.* **79**, 1257–1260.

JIMÉNEZ, J., WRAY, A.A., SAFFMAN, P.G. & ROGALLO, R.S. 1993 The structure of intense vorticity in isotropic turbulence. *J. Fluid. Mech.* **255**, 4, 65–90.

MOISY, F., TABELING, P. & WILLAIME, H. 1999 Kolmogorov Equation in a fully developed turbulence experiment, *Phys. Rev. Lett.* **82** (20), 3994–3997.

MOISY, F. 2000 Etude expérimentale des fluctuations de vitesse, de température et de pression en turbulence développée. *Thesis* Univ. Paris 6.

MOISY, F., ANDERSEN, J.S., WILLAIME, H. & TABELING, P. 2000 Passive scalar intermittency: Statistics of the cliffs, in *Advances in Turbulence VIII* (ed. C. Dopazo) CIMNE Barcelona, 835–838.

MOISY, F. & JIMÉNEZ, J. 2004 Geometry and clustering of intense structures in isotropic turbulence., *J. Fluid. Mech.* **513**, 111–133.

MOURI, H., HORI, A. & KAWASHIMA, Y. 2002 Vortex tubes in velocity fields of laboratory isotropic turbulence: dependence on the Reynolds number. *Phys. Rev. E* **67**, 06305.

OREY, S. 1970 Gaussian sample functions and the Hausdorf dimension of level crossings. *Z. Wahrscheinlichkeitheorie verw. Geb.* **15**, 249–256.

PASSOT, T., POLITANO, H., SULEM, P.L., ANGILELLA, J.R & MENEGUZZI, M. 1995 Instability of strained vortex layers and vortex tube formation in homogeneous turbulence. *J. Fluid. Mech.* **282**, 313–338.

PORTER, D.H., WOODWARD, P.R. & POUQUET, A. 1997 Inertial range structures in decaying compressible turbulent flows, *Phys. Fluids* **10**, 237–245.

PRASKOVSKY, A.A., FOSS, J.F., KLEIS, S.J. & KARYAKIN, M.Y. 1993 Fractal properties of isovelocity surfaces in high Reynolds number laboratory shear flows. *Phys. Fluids A* **5**, 2038–2042.

SCOTTI, A., MENEVEAU, C. & SADDOUGHI, S.G. 1995 Fractal dimension of velocity signals in high-Reynolds-number hydrodynamic turbulence. *Phys. Rev. E* **51** 5594–5608.

SREENIVASAN, K.R. 1991 Fractals and multifractals in fluid turbulence. *Annu. Rev. Fluid Mech.* **23**, 539–600.

SREENIVASAN, K.R. & ANTONIA, R.A. 1997 The phenomenology of small-scale turbulence. *Annu. Rev. Fluid Mech.* **29**, 435–472.

ZOCCHI, G., TABELING, P., MAURER, J., & WILLAIME, H. 1994 Measurement of the scaling of the dissipation at high Reynolds numbers *Phys. Rev. E* **50** (5), 3693–3700.